Modeling and Control of a High-thrust Direct-drive Spiral Motor

Yasutaka Fujimoto, Issam A. Smadi, Hiroko Omori, Koichiro Suzuki, and Hiroshi Hamada
Department of ECE, Yokohama National University, 79-5 Tokiwadai, Yokohama 240-8501, JAPAN

***Abstract*— In this paper, modeling and control of spiral motor is proposed. The voltage equation and motion equation of the spiral motor is proposed. Based on this modeling, control system for the spiral motor is proposed. The proposed controller consists of three parts; the first part is PI current controller with back EMF compensation specialized for spiral motor, the second part is disturbance observer based PD controller for linear and gap motion interacting each other, and the third part is zero-power controller for equilibrium fluctuation of gap displacement. It is confirmed that the proposed controller achieves independent linear position and gap control simultaneously.**

***Index Terms*— Axial flux machine, Linear actuator, Motion control, Robotics.**

I. Introduction

Efficiency and power density of the electric motors are very high compared to other actuators, but its torque is not enough for several applications. Therefore high-ratio gears are combined with electric motors in many applications. Main losses in such actuator systems with the geared servo motors are mechanical transmission loss in the gears, iron loss in the iron core, copper loss in the windings, and switching loss in the power converter. From a control viewpoint, the mechanical loss, i. e., friction loss reduces adaptability, safety, and backdrivability in the motion systems. Various motion mechanisms and controls that recover the backdrivability were reported in the past works[1]–[10].

The authors have proposed a novel helical mechanism of actuator that realizes direct-drive motion without mechanical gears[11]–[13]. The structure and developed prototype are shown in Fig. 1. Permanent magnets are attached on the surfaces of the mover. Slots are provided for winding on the surface of the stator. Three-phase winding in the slots generates flux in the axial direction. Thus, the spiral motor is a helical motion permanent magnet axial flux machine. Due to its large air-gap area, the motor can generate relatively high thrust force.

In this paper, circuit equation and motion equation of the spiral motor are introduced. In order to realize direct-drive motion, we need to keep the air-gap constant. A magnetic levitation control is proposed for this purpose. A variation of the zero power controller is also proposed.

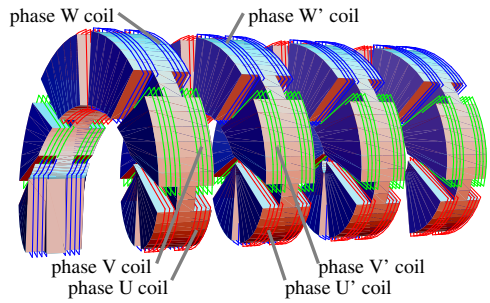

(a) A stator with three-phase windings.

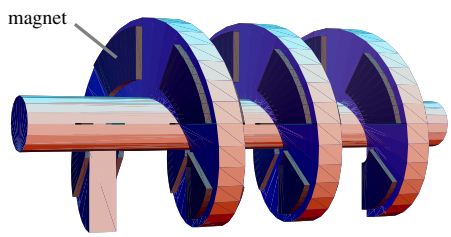

(b) A mover with permanent magnets.

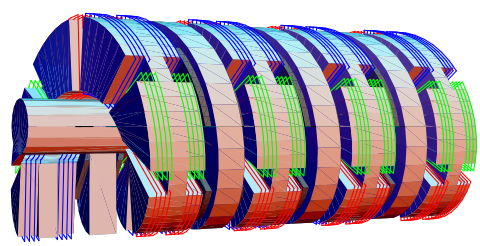

(c) A motor combined with the stator and mover.

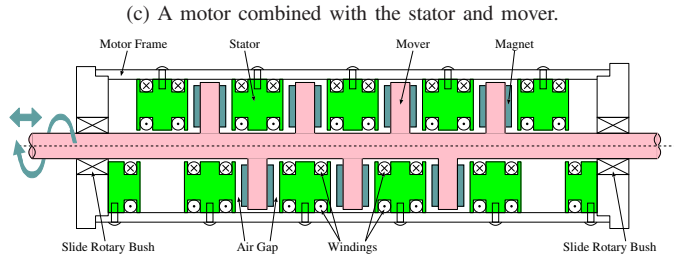

(d) A cross-sectional view.

Fig. 1. A preliminary structure of a spiral motor.

This work was supported by KAKENHI 19676003.

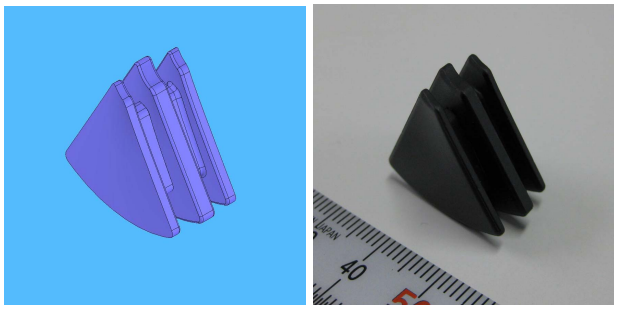

Fig. 2. A helical-shape stator yoke.

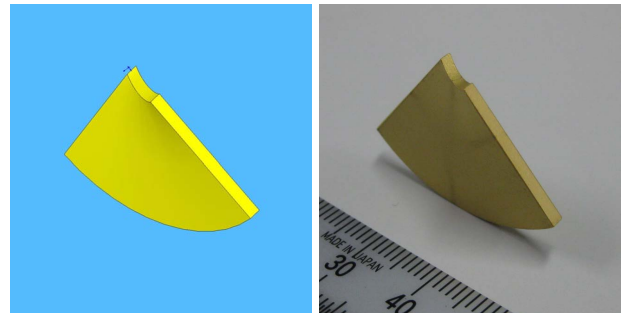

Fig. 3. A helical-shape Nd-Fe-B magnet.

II. Modeling of Spiral Motor

A. Mechanism of Spiral Motor

Figure 1 (a)-(c) shows a preliminary structure of the spiral motor. Permanent magnets are attached on the surfaces of the mover. Slots are provided for windings on the surface of the stator. The spiral motor is a helical motion axial flux permanent magnet motor. Three-phase windings in the slots generates flux in the axial direction. Due to its large air-gap area, the motor can generate relatively high thrust force.

The cross sectional view of the spiral motor is shown in Fig. 1 (d). The radial load applied to the output shaft is supported by two slide rotary bushes and the thrust load is directly controlled by the electromagnetic force. Thus a magnetic levitation control is required to keep the air-gap constant. For this levitation control, two independent three-phase inverters are required.

B. Prototypes

Four types of prototype of spiral motors have been developed as shown in Table III. A helical-shape stator yoke is made of soft magnetic composite (SMC) as shown in Fig. 2. A helical-shape magnet is made of Nd-Fe-B as shown in Fig. 3. Internal structure of the stator is shown in Fig. 4. The Nd-Fe-B magnets are attached on the mover yoke which is made of silicon steel, as shown in Fig. 5. Precise helical shapes of the stator and mover enable uniform short length of air-gap and avoid concentration of stress when the mover touches down to the stator.

Exterior of the spiral motor is shown in Fig. 6. A rotary encoder and linear encoder attached at the mover measure the linear position x and rotation angle θ for control. Displacement of the air gap x_g is computed by using these measurement as follows.

$$x_g = x - \frac{\ell_p}{2\pi}\theta \tag{1}$$

C. Permeance Model

In order to derive analytical voltage equation, and thrust-force and torque equations, a permeance model of the motor for 360 degree electric angular displacement in polar coordinates is presented.

Figure 7 shows the polar coordinates expression of the motor. From this model, a simple magnetic circuit as shown in Fig. 8 is obtained. For simplicity magnetic resistance of the iron core is ignored. $R_g = 3p(\ell_g - x_g)/S\mu_0$ is magnetic resistance of forward side air gap for an area of each phase windings, where S is a gap area of the cross section of the cylinder. $R'_g = 3p(\ell_g + x_g)/S\mu_0$ is magnetic resistance of backward side air gap. $R_m = 3p\ell_m/S\mu_m$ is magnetic resistance of a permanent magnet. $c(\cdot)I_f$ is a spatial function of magnetomotive force of the field magnet by the permanent magnet and approximated by a cosine function as $c(\theta) = k\cos(\theta)$ where $k = \frac{6\sqrt{3}}{\pi^2}\sin(p\alpha/2)$ is the fundamental component of $c(\theta)$. $I_f = B_r\ell_m/\mu_m$ is an equivalent magnetization current, i. e., magnetomotive force of the permanent magnet. These parameters are shown in Table II. For simplicity, we assume that the permeability of the permanent magnet μ_m is equivalent to μ_0. Also the edge effect is ignored.

In the part (A) of the magnetic circuit, interlinkage flux $\Phi = [\Phi_u, \Phi_v, \Phi_w, \Phi_f]^T$ for each current is obtained as $\Phi = LI$ where $I = [I_u, I_v, I_w, I_f]^T$ is current vector and L is an inductance matrix:

$$L = P\begin{bmatrix} n^2 & -\frac{1}{2}n^2 & -\frac{1}{2}n^2 & \frac{3}{2}nkc_0 \\ -\frac{1}{2}n^2 & n^2 & -\frac{1}{3}n^2 & \frac{3}{2}nkc_1 \\ -\frac{1}{2}n^2 & -\frac{1}{2}n^2 & n^2 & \frac{3}{2}nkc_2 \\ \frac{3}{2}nkc_0 & \frac{3}{2}nkc_1 & \frac{3}{2}nkc_2 & (\frac{3k}{2})^2 \end{bmatrix} \tag{2}$$

TABLE I

Specifications of spiral motors.

	#1	#2	#3	#4
Number of stator layers	6	8.5	12	12
Number of mover layers	2	4	7	5
Length of flame*[mm]	132	182	252	252
Diameter of flame*[mm]	55	55	55	55
Stroke[mm]	60	70	80	120
Lead length of screw[mm]	20	20	20	20
Nominal length of air gap[mm]	1	1	1	1

*excluding projecting parts

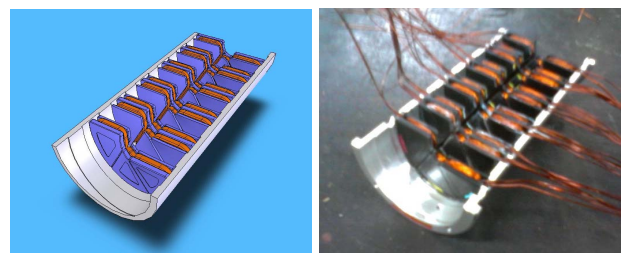

Fig. 4. Internal structure of a stator. (model #1)

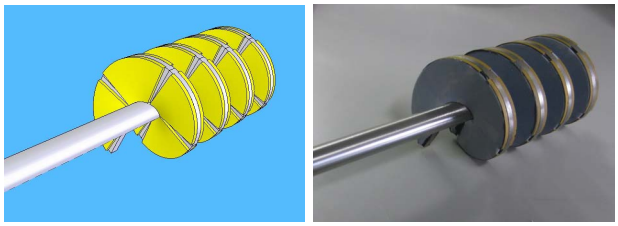

Fig. 5. A mover. (model #2)

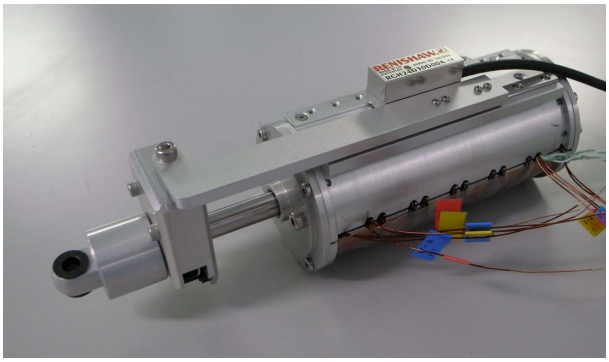

Fig. 6. Exterior of a spiral motor. (model #1)

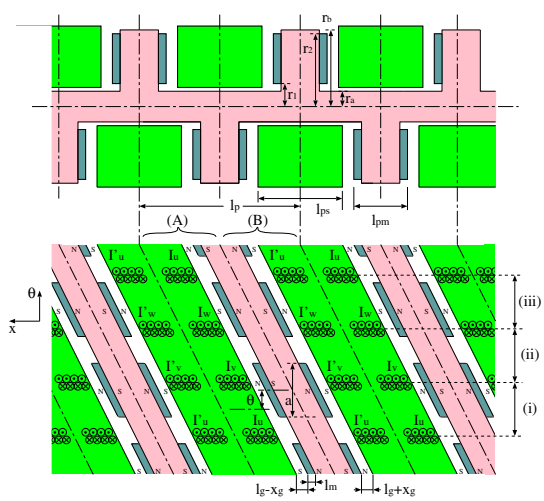

Fig. 7. A spiral motor in polar coordinates.

where $P = \frac{2}{3(R_g+R_m)}$ is permeance for one-phase current and $c_i = \cos(p\theta - \frac{2i\pi}{3})$.

In general, a salient-mover machine has a mutual inductance between n_i-turns windings at position θ_i and n_j-turns windings at position θ_j represented by

$$\begin{aligned} L_{ij} &= P_d n_i n_j \cos(\theta_i - p\theta)\cos(\theta_j - p\theta) \\ &\quad + P_q n_i n_j \sin(\theta_i - p\theta)\sin(\theta_j - p\theta) \end{aligned} \tag{3}$$

where $P_d \propto 1/(\ell - x_g)$ is d-axis permeance and $P_q \propto 1/(\ell - x_g)$ is q-axis permeance. $\ell = \ell_g + \ell_m$ is a nominal gap between the mover iron and the stator. Instead of (2), we

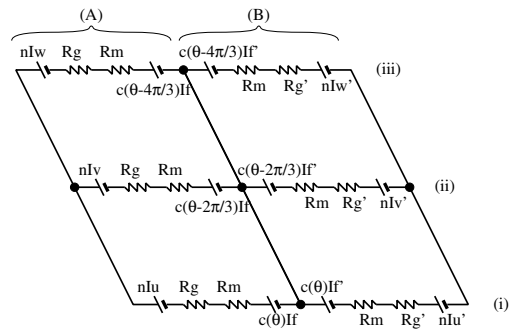

Fig. 8. A magnetic circuit.

TABLE II
NOMENCLATURE

α	angle of a sector-type permanent magnet
B_r	residual flux density of a permanent magnet
f	thrust force of the mover
I_f	magnetomotive force of a field magnet
I_i	i-axis current on forward side windings, $i \in \{d, q\}$
I'_i	i-axis current on backward side windings, $i \in \{d, q\}$
J	moment of inertia of the mover around the axis
k	a fundamental Fourier component of $c(\theta)$
ℓ	a nominal gap between the mover iron and the stator
ℓ_g	nominal length of air gap
ℓ_m	thickness of magnet
ℓ_p	lead length of screw
μ_0	the permeability in vacuum
μ_m	permeability of a permanent magnet
M	mass of the mover
n	ampere-turn
p	number of pole pairs per 360 degree mechanical angular displacement
q	number of layers
θ	mechanical rotational angle of the mover
S	a gap area per 360 degree mechanical angle displacement
τ	torque of the mover
x	a linear position of the mover
x_g	displacement of air gap

adopt a inductance matrix as follows

$$L = \begin{bmatrix} L_{00} & L_{01} & L_{02} & L_{03} \\ L_{10} & L_{11} & L_{12} & L_{13} \\ L_{20} & L_{21} & L_{22} & L_{23} \\ L_{30} & L_{31} & L_{32} & L_{33} \end{bmatrix} \tag{4}$$

where $n_0 = n_1 = n_2 = n$, $n_3 = n_f = 3k/2$, $\theta_0 = 0$, $\theta_1 = 2\pi/3$, $\theta_2 = 4\pi/3$, and $\theta_3 = p\theta$. The model (4) is equivalent to (2) if the machine is not salient, i. e., $P_d = P_q = P$ holds.

The voltage equation, thrust-force equation, and torque equation of the spiral motor are derived by using the inductance matrix (4) as follows.

$$V = RI + L\frac{dI}{dt} + \dot{\theta}\frac{\partial L}{\partial \theta}I + \dot{x}\frac{\partial L}{\partial x}I \tag{5}$$

$$f = \frac{1}{2}I^T\frac{\partial L}{\partial x}I \tag{6}$$

$$\tau = \frac{1}{2}I^T\frac{\partial L}{\partial \theta}I \tag{7}$$

where $V = [V_u, V_v, V_w, V_f]^T$ is voltage of each windings,

$R = \mathrm{diag}(R_s, R_s, R_s, R_f)$ is resistance of windings, and f and τ are thrust-force and torque of the mover, respectively.

D. Voltage Equation on dq-axis

In order to apply field oriented control to the spiral motor, dq-axis model of the spiral motor is derived as follows. Let the transformation matrix C be

$$C = \begin{bmatrix} \sqrt{\frac{2}{3}}c_0 & \sqrt{\frac{2}{3}}c_1 & \sqrt{\frac{2}{3}}c_2 & 0 \\ -\sqrt{\frac{2}{3}}s_0 & -\sqrt{\frac{2}{3}}s_1 & -\sqrt{\frac{2}{3}}s_2 & 0 \\ \frac{1}{\sqrt{3}} & \frac{1}{\sqrt{3}} & \frac{1}{\sqrt{3}} & 0 \\ 0 & 0 & 0 & 1 \end{bmatrix} \quad (8)$$

where $c_i = \cos(p\theta - \frac{2i\pi}{3})$, $s_i = \sin(p\theta - \frac{2i\pi}{3})$. Then the dq-axis current and voltage are represented by $I_{dq} = CI$ and $V_{dq} = CV$ where $I_{dq} = [I_d, I_q, I_0, I_f]^T$, $V_{dq} = [V_d, V_q, V_0, V_f]^T$. And I_d, I_q, I_0 are d-axis, q-axis, and zero-phase current, V_d, V_q, V_0 are d-axis, q-axis, and zero-phase voltage, respectively.

The voltage equation on dq-axis is

$$\begin{aligned} V_{dq} &= CRC^T I_{dq} + CLC^T \dot{I}_{dq} + \dot{\theta} C \frac{\partial L}{\partial \theta} C^T I_{dq} \\ &\quad + \dot{\theta} CL \frac{\partial C^T}{\partial \theta} I_{dq} + \dot{x} C \frac{\partial L}{\partial x} C^T I_{dq} \end{aligned} \quad (9)$$

In (9), note that

$$\begin{aligned} \frac{\partial L}{\partial \theta} &= \left. \frac{\partial L(x_g, \theta)}{\partial \theta} \right|_{x_g = x - \frac{\ell_p}{2\pi}\theta} \\ &= \frac{\partial L(x_g, \theta)}{\partial \theta} - \frac{\ell_p}{2\pi} \frac{\partial L(x_g, \theta)}{\partial x_g} \end{aligned} \quad (10)$$

Then, the voltage equation (9) is expanded as follows.

$$\begin{aligned} V_d &= R_s I_d + L_d \dot{I}_d - p\dot{\theta} L_q I_q + L_{df} \dot{I}_f \\ &\quad + \frac{\dot{x}_g}{\ell - x_g}(L_d I_d + L_{df} I_f) \quad (11) \\ V_q &= R_s I_q + L_q \dot{I}_q + p\dot{\theta}(L_d I_d + L_{df} I_f) \\ &\quad + \frac{\dot{x}_g}{\ell - x_g} L_q I_q \quad (12) \\ V_0 &= R_s I_0 \quad (13) \\ V_f &= L_f \dot{I}_f + L_{df} \dot{I}_d + \frac{\dot{x}_g}{\ell - x_g}(L_d I_f + L_{df} I_d) \quad (14) \end{aligned}$$

where $L_d = \frac{3}{2} n^2 P_d \propto 1/(\ell - x_g)$ and $L_q = \frac{3}{2} n^2 P_q \propto 1/(\ell - x_g)$ are d-axis and q-axis inductances, respectively. $L_{df} = \sqrt{\frac{3}{2}} n n_f P_d \propto 1/(\ell - x_g)$ is equivalent mutual inductance between d-axis stator windings and field magnet windings. $L_f = n_f^2 P_d \propto 1/(\ell - x_g)$ is equivalent self-inductance of field magnet windings.

Finally, following dq-axis voltage equation is obtained by taking first two equations (11), (12) and substituting $\dot{I}_f = 0$.

$$\begin{aligned} \begin{bmatrix} V_d \\ V_q \end{bmatrix} &= \begin{bmatrix} R_s + L_d(\frac{d}{dt}) & 0 \\ 0 & R_s + L_q(\frac{d}{dt}) \end{bmatrix} \begin{bmatrix} I_d \\ I_q \end{bmatrix} + \Psi_f \begin{bmatrix} \frac{1}{\ell - x_g}\dot{x}_g \\ p\dot{\theta} \end{bmatrix} \\ &\quad + \frac{\dot{x}_g}{\ell - x_g} \begin{bmatrix} L_d & 0 \\ 0 & L_q \end{bmatrix} \begin{bmatrix} I_d \\ I_q \end{bmatrix} + p\dot{\theta} \begin{bmatrix} 0 & -L_q \\ L_d & 0 \end{bmatrix} \begin{bmatrix} I_d \\ I_q \end{bmatrix} \end{aligned} \quad (15)$$

where $\Psi_f = L_{df} I_f$ corresponds to field flux by the permanent magnet. Fig. 9 shows block diagram of this dq-axis circuit model.

As the same manner, voltage equation of part (B) in Fig. 7 and 8 is obtained as follows.

$$\begin{aligned} \begin{bmatrix} V'_d \\ V'_q \end{bmatrix} &= \begin{bmatrix} R_s + L'_d(\frac{d}{dt}) & 0 \\ 0 & R_s + L'_q(\frac{d}{dt}) \end{bmatrix} \begin{bmatrix} I'_d \\ I'_q \end{bmatrix} + \Psi'_f \begin{bmatrix} -\frac{1}{\ell + x_g}\dot{x}_g \\ p\dot{\theta} \end{bmatrix} \\ &\quad - \frac{\dot{x}_g}{\ell + x_g} \begin{bmatrix} L'_d & 0 \\ 0 & L'_q \end{bmatrix} \begin{bmatrix} I'_d \\ I'_q \end{bmatrix} + p\dot{\theta} \begin{bmatrix} 0 & -L'_q \\ L'_d & 0 \end{bmatrix} \begin{bmatrix} I'_d \\ I'_q \end{bmatrix} \end{aligned} \quad (16)$$

where $L'_d = \frac{3}{2} n^2 P'_d \propto 1/(\ell + x_g)$ and $L'_q = \frac{3}{2} n^2 P'_q \propto 1/(\ell + x_g)$ are d-axis and q-axis inductances in part (B), respectively. $\Psi'_f = L'_{df} I'_f$ corresponds to field flux by the permanent magnet in part (B), where $L'_{df} = \sqrt{\frac{3}{2}} n n_f P'_d \propto 1/(\ell + x_g)$.

Two independent three-phase inverters are required for driving the spiral motor. One inverter controls the circuit (15) and the other controls the circuit (16).

E. Thrust-force/Torque Equation

Thrust-force equation (6) and torque equation (7) are rewritten by using I_{dq} as follows.

$$\begin{aligned} f &= \frac{1}{2} I_{dq}^T C \frac{\partial L}{\partial x} C^T I_{dq} \quad (17) \\ &= \frac{1}{\ell - x_g} \left(\Psi_f I_d + \frac{L_d I_d^2 + L_q I_q^2 + L_f I_f^2}{2} \right) \quad (18) \\ \tau &= \frac{1}{2} I_{dq}^T C \frac{\partial L}{\partial \theta} C^T I_{dq} \quad (19) \\ &= p(\Psi_f I_q + (L_d - L_q) I_d I_q) \\ &\quad - \frac{\ell_p}{2\pi} \frac{1}{\ell - x_g} \left(\Psi_f I_d + \frac{L_d I_d^2 + L_q I_q^2 + L_f I_f^2}{2} \right) \quad (20) \end{aligned}$$

As the same manner, thrust-force equation and torque equation in part (B) are obtained as follows.

$$\begin{aligned} f' &= -\frac{1}{\ell + x_g} \left(\Psi'_f I'_d + \frac{L'_d I'^2_d + L'_q I'^2_q + L'_f I'^2_f}{2} \right) \quad (21) \\ \tau' &= p(\Psi'_f I'_q + (L'_d - L'_q) I'_d I'_q) \\ &\quad + \frac{\ell_p}{2\pi} \frac{1}{\ell + x_g} \left(\Psi'_f I'_d + \frac{L'_d I'^2_d + L'_q I'^2_q + L'_f I'^2_f}{2} \right) \quad (22) \end{aligned}$$

Finally, total thrust-force and torque per 360 degree electrical angle are obtained as $f_{total} = f + f'$ and $\tau_{total} = \tau + \tau'$. Hense, the equation of motion is obtained as follows.

$$\begin{aligned} M\ddot{x} &= pq(f + f') - D\dot{x} - d \quad (23) \\ J\ddot{\theta} &= pq(\tau + \tau') - D_\tau \dot{\theta} - d_\tau \quad (24) \end{aligned}$$

where M, J are mass and inertia of the mover, respectively. D, D_τ are friction coefficient for linear and rotaty motion, respectively. d, d_τ are disturbance force and torque applied to the mover, respectively.

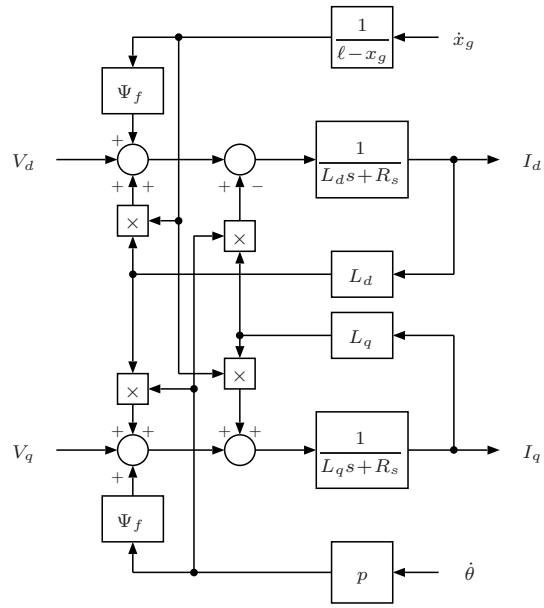

Fig. 9. dq-axis circuit model of the spiral motor in part A.

F. Simplified Thrust-Force/Torque Model

For control design, a simplified model is obtained by linearlizing (18), (20), (21), and (22) around $x_g = 0$.

$$\begin{aligned} f_{total} &\simeq \frac{2L_{f0}I_f^2}{\ell^2}x_g + \frac{\Psi_{f0}}{\ell}(I_d - I_d') \\ &\quad + \frac{L_{d0}}{2\ell}(I_d^2 - I_d'^2) + \frac{L_{q0}}{2\ell}(I_q^2 - I_q'^2) \qquad (25) \\ \tau_{total} &\simeq p\left(\Psi_{f0}(I_q + I_q') + (L_{d0} - L_{q0})(I_d I_q + I_d' I_q')\right) \\ &\quad - \frac{\ell_p}{2\pi}\left(\frac{2L_{f0}I_f^2}{\ell^2}x_g + \frac{\Psi_{f0}}{\ell}(I_d - I_d')\right. \\ &\quad \left. + \frac{L_{d0}}{2\ell}(I_d^2 - I_d'^2) + \frac{L_{q0}}{2\ell}(I_q^2 - I_q'^2)\right) \qquad (26) \end{aligned}$$

where $L_{d0} = L_d|_{x_g=0} = L_d'|_{x_g=0}$, $L_{q0} = L_q|_{x_g=0} = L_q'|_{x_g=0}$, $\Psi_{f0} = \Psi_f|_{x_g=0} = \Psi_f'|_{x_g=0}$, and $L_{f0} = L_f|_{x_g=0} = L_f'|_{x_g=0}$.

From (25) and (26), linear motion is mainly controlled by d-axis current and rotational motion is mainly controlled by q-axis current. The first term in (25) corresponds to a unstable drift force which is a positive feedback in terms of gap displacement.

When the field oriented control is applied to (15) and (16) and their current hold conditions $I_d = -I_d'$ and $I_q = I_q'$ by the current control, then we have

$$\begin{aligned} f_{total} &\simeq K_g x_g + K_f I_d \qquad (27) \\ \tau_{total} &\simeq K_\tau I_q - \frac{\ell_p}{2\pi}(K_g x_g + K_f I_d) \qquad (28) \end{aligned}$$

where $K_g = \frac{2L_{f0}I_f^2}{\ell^2}$, $K_f = \frac{2\Psi_{f0}}{\ell}$, and $K_\tau = 2p\Psi_{f0}$. From (23), (24), (27), and (28), it turns out that the motion system has a spring whose coefficient is negative. Figure 10 shows the block diagram of the simplified model of the motion system.

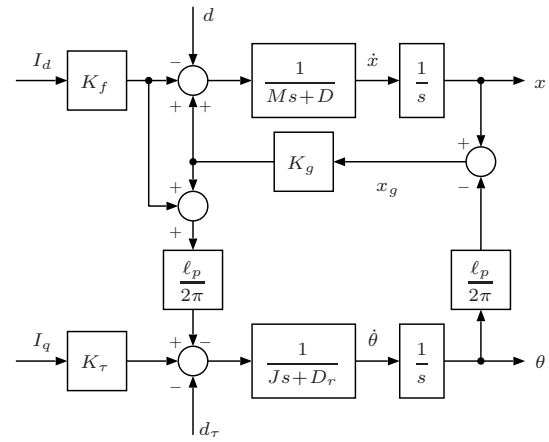

Fig. 10. Simplified motion model of the spiral motor.

III. Control of the Spiral Motor

A. Current Controller

From (15) and (16), current controller is designed as follows.

$$\begin{aligned} V_d^{ref} &= \left(K_{pd} + \frac{K_{id}}{s}\right)(I_d^{ref} - I_d) + \hat{E}_d \qquad (29) \\ V_q^{ref} &= \left(K_{pq} + \frac{K_{iq}}{s}\right)(I_q^{ref} - I_q) + \hat{E}_q \qquad (30) \\ V_d'^{ref} &= \left(K_{pd} + \frac{K_{id}}{s}\right)(-I_d^{ref} - I_d') + \hat{E}_d' \qquad (31) \\ V_q'^{ref} &= \left(K_{pq} + \frac{K_{iq}}{s}\right)(I_q^{ref} - I_q') + \hat{E}_q' \qquad (32) \end{aligned}$$

where the controller gains are chosen so that $K_{pd} = \omega_{id}L_{d0}$, $K_{pq} = \omega_{iq}L_{q0}$, $K_{id} = \omega_{id}R_s$, and $K_{iq} = \omega_{iq}R_s$. Also $\hat{E}_d$, $\hat{E}_q$, $\hat{E}_d'$, and $\hat{E}_q'$ are back EMF compensation given by

$$\begin{aligned} \hat{E}_d &= \frac{\dot{x}_g}{\ell}(\Psi_{f0} + L_{d0}I_d) - p\dot{\theta}L_{q0}I_q \qquad (33) \\ \hat{E}_q &= p\dot{\theta}(\Psi_{f0} + L_{d0}I_d) + \frac{\dot{x}_g}{\ell}L_{q0}I_q \qquad (34) \\ \hat{E}_d' &= -\frac{\dot{x}_g}{\ell}(\Psi_{f0} + L_{d0}I_d') - p\dot{\theta}L_{q0}I_q' \qquad (35) \\ \hat{E}_q' &= p\dot{\theta}(\Psi_{f0} + L_{d0}I_d') - \frac{\dot{x}_g}{\ell}L_{q0}I_q'. \qquad (36) \end{aligned}$$

B. Position/Gap Controller with Disturbance Observer

From (27) and (28), current references are obtained as follows.

$$\begin{aligned} I_d^{ref} &= \frac{1}{K_f}(f^{ref} - K_g x_g) \qquad (37) \\ I_q^{ref} &= \frac{1}{K_\tau}\left(\frac{\ell_p}{2\pi}f^{ref} + \tau^{ref}\right) \qquad (38) \end{aligned}$$

where f^{ref} and τ^{ref} correspond to thrust-force and torque references. The modeling error and disturbance are compensated by using disturbance observer[2] as follows.

$$\begin{aligned} f^{ref} &= M_n\ddot{x}^{ref} + \hat{d} \qquad (39) \\ \tau^{ref} &= J_n\ddot{\theta}^{ref} + \hat{d}_\tau \qquad (40) \end{aligned}$$

where the terms $\hat{d}$ and $\hat{d}_\tau$ are estimated disturbandes.

$$\hat{d} = \frac{\omega_d}{s+\omega_d}(f^{ref} - M_n s\dot{x}) \quad (41)$$

$$\hat{d}_\tau = \frac{\omega_d}{s+\omega_d}(\tau^{ref} - J_n s\dot{\theta}) \quad (42)$$

The acceleration references in (39) and (40) are computed by trajectory tracking feedback controller for position x and regulator for gap displacement x_g as follows.

$$\ddot{x}^{ref} = K_{px}(x^{cmd} - x) + K_{dx}(\dot{x}^{cmd} - \dot{x}) + \ddot{x}^{cmd} \quad (43)$$

$$\ddot{x}_g^{ref} = K_{pg}(x_g^{cmd} - x_g) + K_{dg}(\dot{x}_g^{cmd} - \dot{x}_g) \quad (44)$$

$$\ddot{\theta}^{ref} = \frac{2\pi}{\ell_p}(\ddot{x}^{ref} - \ddot{x}_g^{ref}) \quad (45)$$

where x^{cmd} represents position command of the mover, x_g^{cmd} represents gap displacement command, respectively. Ideally, the unstable equilibrium point corresponds to being the gap displacement $x_g = 0$. However, there is a offset of the equilibrium point according to the manufacturing accuracy of the parts of the stator and mover. Thrust load also affects the offset. In such a case, there remains constant current in order to achieve $x_g = 0$, which causes copper loss in the windings. x_g^{cmd} should be set to be the equilibrium point by using the zero power controller.

C. Zero Power Controller

Zero-power control[14] was proposed for electromagnetic suspension systems using permanent magnets, which achieves automatic gap adjustment so that the input current converges to zero. In this paper, we propose a variation of zero-power controller suitable for our control system.

The equilibrium gap displacement x_g^{cmd} in (44) is obtained by integrating d-axis current reference I_d^{ref} as follows. x_g^{cmd} approaches to the equilibrium point and finally $I_d = 0$ is achieved if x_g^{cmd} corresponds to the equilibrium.

$$x_g^{cmd} = \frac{K_z}{s} I_d^{ref} \quad (46)$$

$$\dot{x}_g^{cmd} = K_z I_d^{ref} \quad (47)$$

where K_z represents a controller gain.

D. Overall Control System

Finally, the overall control system of the spiral motor is described as shown in Fig. 11.

IV. Simulation

A. Plant and Control Parameters

Table III shows plant and control parameters. The electrical plant parameters in this table are for 360 degree electrical angle.

TABLE III
PLANT AND CONTROL PARAMETERS

p	number of pole pairs per 360 degree	2
q	number of layers	2
ℓ_g	nominal length of air gap	1 [mm]
ℓ_m	thickness of magnet	2 [mm]
B_r	residual flux density of magnet	1.2 [T]
n	ampere-turn	50
R_s	registance of windings	0.374 [Ω]
L_{d0}	nominal d-axis inductance	0.329 [mH]
L_{q0}	nominal q-axis inductance	0.329 [mH]
Ψ_{f0}	nominal field flux	0.0195 [Wb]
K_f	thrust-force constant	13.0 [N/A]
K_τ	torque constant	0.0781 [N.m/A]
J	moment of inertia of the mover	715 [g cm^2]
M	mass of the mover	0.229 [kg]
K_g	equivalent spring coefficient	25800 [N/m]
K_{pd}, K_{pq}	propotional gain of current controller	1.64
K_{id}, K_{iq}	integral gain of current controller	1870
ω_{id}, ω_{iq}	bandwidth of current control system	5000 [rad/sec]
ω_d	bandwidth of disturbance observer	500 [rad/s]
K_{px}	propotional gain of position controller	10000
K_{dx}	derivative gain of position controller	200
ω_x	bandwidth of position control system	100 [rad/sec]
K_{pg}	propotional gain of position controller	2500
K_{dg}	derivative gain of position controller	100
ω_g	bandwidth of gap control system	50 [rad/sec]
K_z	gain of zero-power controller	0.002
V_{dc}	dc link voltage of inverter	80 [V]
T_s	control sampling period	50 [μsec]
Δx	resolution of linear encoder with quad edge evaluation method	0.25 [μm]
$\Delta\theta$	resolution of rotary encoder with quad edge evaluation method	2π/20000 [rad]

B. Results

The proposed control system is applied to spiral motor model (5)–(7). Figure 12 shows simulation results of the proposed control. The mover touches down at $t = 0$[sec], i. e., the gap displacement is set to $x_g = 0.7$[mm] as the initial condition. Step command $x^{cmd} = 1$[mm] for the linear position x is given at $t = 0.4$[sec]. Figure 12(a) shows the position and gap response of the mover. In this figure, the rotation angle θ is converted to equivalent linear displacement by multiplying $\ell_p/2\pi$. We can see that the gap displacement converges to neutral position and the mover position converges to the command value without interfaring gap control. Fig. 12(b)(c) show armature current and input voltage on dq-axis.

C. Response under Inertia Fluctuation

Figure 13 shows simulation results when the actual mass M fluctuates 10 times bigger than the nominal value M_n. Very robust response is obtained.

D. Response under Equilibrium Fluctuation

Figure 14–15 show simulation results under equilibrium fluctuation. The offset of equilibrium is set at $x_g = 50$[μm]. Figure 14 is a case with the proposed zero-power controller. The gap displacement converges to equilibrium point and zero current is realized. On the other hand, in a case without the proposed zero-power controller as shown in Fig. 15, the gap controller manages to keep $x_g = 0$ where continuous

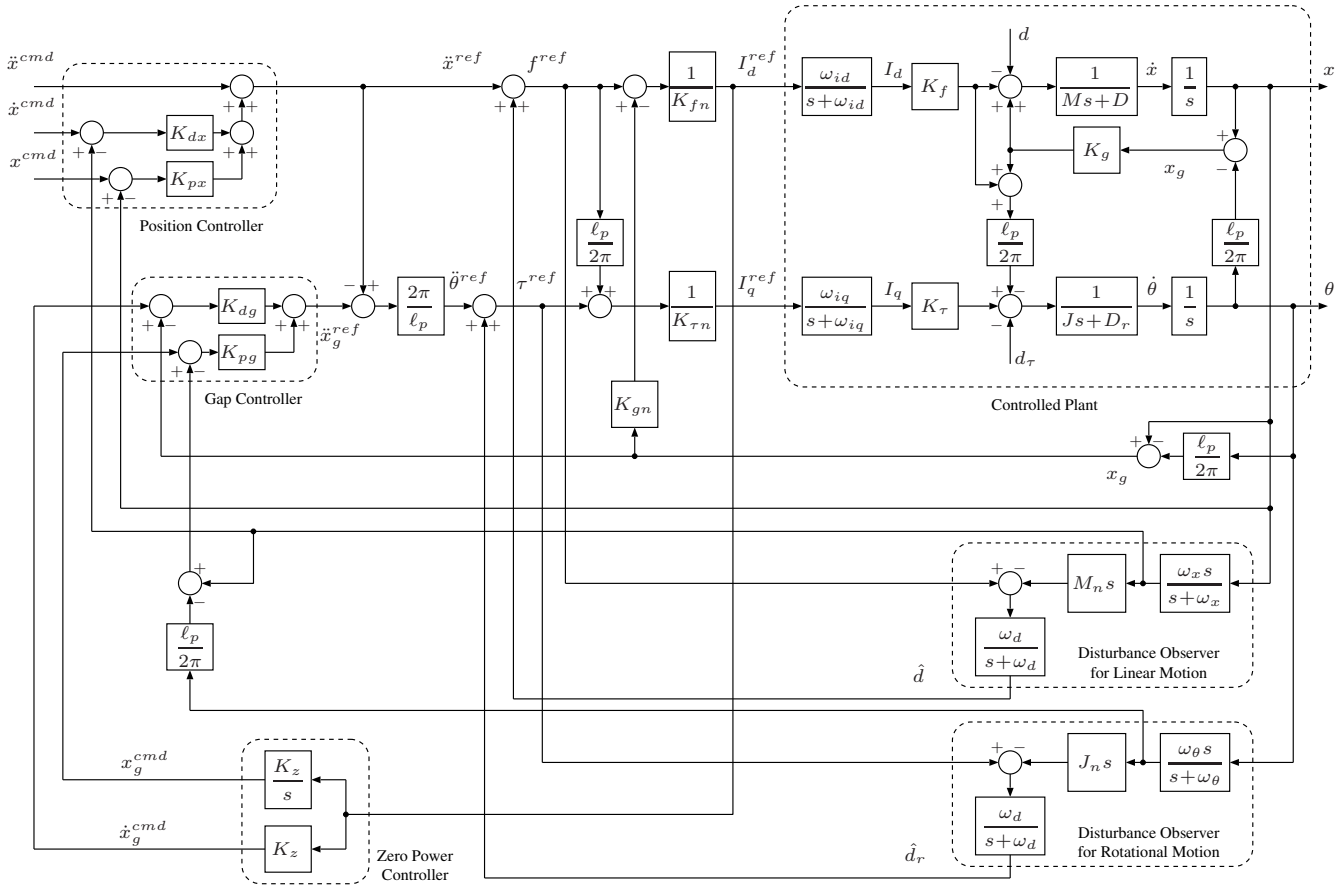

Fig. 11. Overall control system of spiral motor.

current required. Positioning accuracy of both cases are almost same. Thus, the proposed control has a advantage of energy efficiency.

V. Conclusion

In this paper, modeling and control of spiral motor is proposed. The model consists of two parts; one is voltage equation that is an extension of well-known dq-axis model, and the other is motion equation that has a negative spring. The proposed controller consists of three parts; the first part is PI current controller with back EMF compensation specialized for spiral motor, the second part is disturbance observer based PD controller for linear and gap motion interacting each other, and the third part is zero-power controller for equilibrium fluctuation of gap displacement. It is comfirmed that the proposed controller achieves independent linear position and gap control simultaneously.

References

[1] H. Asada and T. Kanade, "Design of direct-drive mechanical arms," *ASME J. of Vibration, Stress, and Reliability in Design*, vol. 105, no. 3, pp. 312–316, 1983.

[2] T. Murakami, F. Yu, and K. Ohnishi, "Torque sensorless control in multidegree-of-freedom manipulator," *IEEE Trans. Industrial Electronics*, vol. 40, no. 2, pp. 259–265, 1993.

[3] S. Katsura, Y. Matsumoto, and K. Ohnishi, "Analysis and experimental validation of force bandwidth for force control," *IEEE Trans. Industrial Electronics*, vol. 53, no. 3, pp. 922–928, 2006.

[4] S. Katsura, Y. Matsumoto, and K. Ohnishi, "Modeling of force sensing and validation of disturbance observer for force control," *IEEE Trans. Industrial Electronics*, vol. 54, no. 1, pp. 530–538, 2007.

[5] S. Katsura, K. Irie, and K. Ohishi, "Wideband force control by position-acceleration integrated disturbance observer," *IEEE Trans. Industrial Electronics*, vol. 55, no. 4, pp. 1699–1706, 2008.

[6] N. Hayashida, T. Yakoh, T. Murakami, and K. Ohnishi, "A sensorless force control in twin drive systems," in *Proc. IEEE IECON*, pp. 2231–2236, 2000.

[7] G. Pratt and M. Williamson, "Series elastic actuators," in *Proc. IEEE IROS*, pp 399–406, 1995.

[8] M. Zinn, O. Khatib, B. Roth, J. K. Salisbury, "Playing it safe," *IEEE Robotics and Automation Magazine*, vol. 11, no. 2, pp. 12–21, 2004.

[9] A. Bicchi and G. Tonietti, "Fast and "soft-arm" tactics," *IEEE Robotics and Automation Magazine*, vol. 11, no. 2, pp. 22–33, 2004.

[10] A. Bicchi, M. Bavaro, G. Boccadamo, D. De Carli, R. Filippini, G. Grioli, M. Piccigallo, G. Tonietti, R. Schiavi, and S. Sen, "Physical human-robot interaction: dependability, safety, and performance," in *Proc. IEEE AMC*, pp. 9–14, 2008.

[11] Y. Fujimoto, T. Kominami, and H. Hamada, "Development and analysis of a high thrust force direct-drive linear actuator," *IEEE Trans. Industrial Electronics*, vol. 56, no. 5, pp. 1383–1392, 2009.

[12] Y. Fujimoto, Y. Wakayama, H. Ohmori, and I. A. Smadi, "On a High-Backdrivable Direct-drive Actuator for Musculoskeletal Bipedal Robots," in *proc. IEEE AMC*, NF-003891, 2010.

[13] I. A. Smadi, H. Ohmori, and Y. Fujimoto, "On Independent Position/Gap Control of a Spiral Motor," in *proc. IEEE AMC*, NF-001899, 2010.

[14] M. Morishita, M. Akashi, and T. Azukizawa, "Zero-power Control for Maglev System of A Rigid Body Vehicle with Multi-suspended Points," IEEJ Trans. on Industry Applications, vol. 120-D, no. 4, pp. 509-519, 2000.

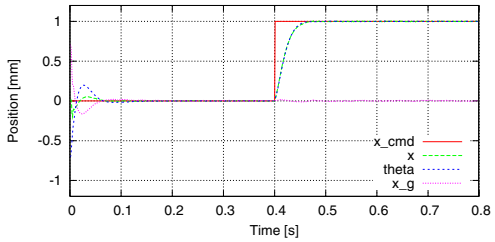

(a) Position and angle of the mover and gap displacement.

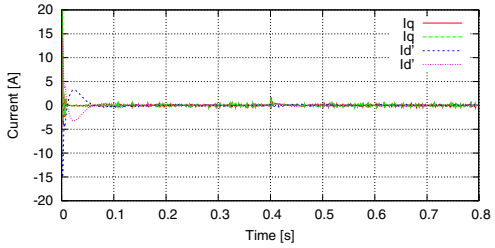

(b) Armature current.

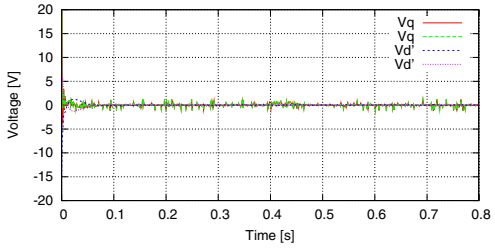

(c) Input voltage.

Fig. 12. Simulation results.

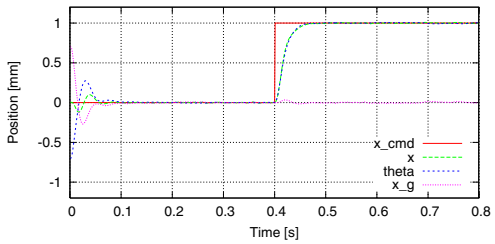

(a) Position and angle of the mover and gap displacement.

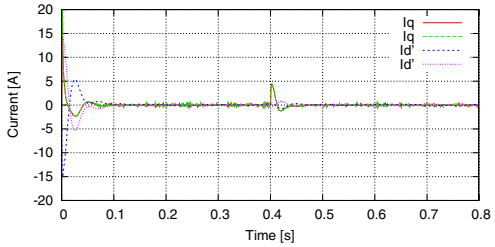

(b) Armature current.

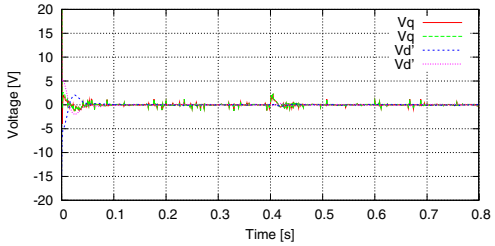

(c) Input voltage.

Fig. 13. Simulation results with mass fluctuation. ($M = 10M_n$)

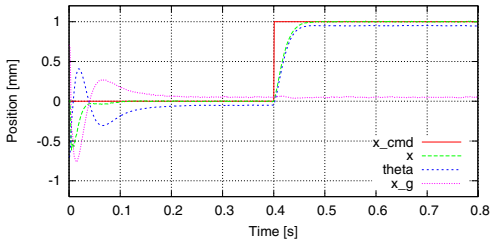

(a) Position and angle of the mover and gap displacement.

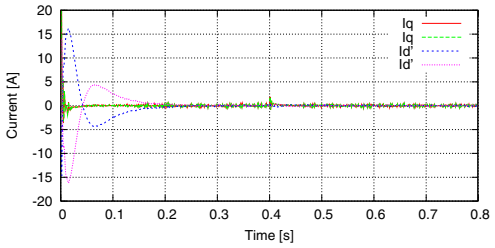

(b) Armature current.

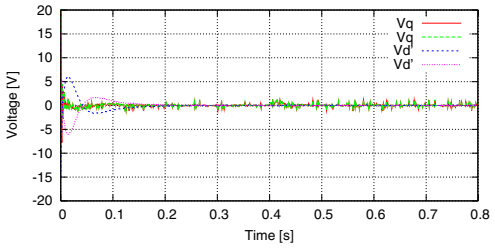

(c) Input voltage.

Fig. 14. Simulation results with equilibrium fluctuation. (offset = 50 [μm])

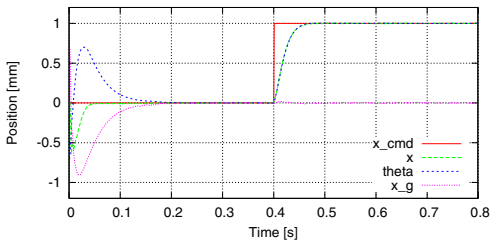

(a) Position and angle of the mover and gap displacement.

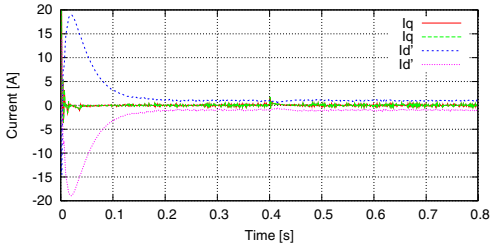

(b) Armature current.

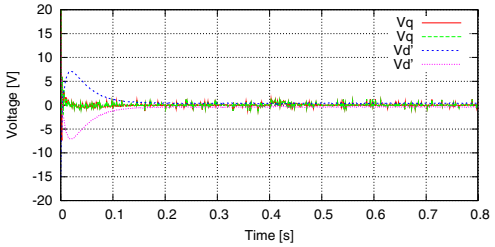

(c) Input voltage.

Fig. 15. Simulation results with equilibrium fluctuation without zero-power controller. (offset = 50 [μm])